Supporting Information

Strategic siting and grid interconnections key to low-carbon future in African countries

Grace C. Wu*[1,2], Ranjit Deshmukh†[1,2], Kudakwashe Ndhlukula[3], Tijana Radojicic[4], Jessica Reilly-Moman[1], Amol Phadke[2], Daniel M. Kammen[1] and Duncan S. Callaway[1]

[1]Energy and Resources Group, University of California at Berkeley, CA 94720, USA
[2]International Energy Studies Group, Lawrence Berkeley National Laboratory, CA 94720, USA
[3]Southern Africa Development Community (SADC) Centre for Renewable Energy and Energy Efficiency, Namibia University of Science and Technology, Windhoek, Namibia
[4]International Renewable Energy Agency, Abu Dhabi, UAE

Contents

*grace.cc.wu@berkeley.edu
†rdeshmukh@lbl.gov

SI Text

S1 Materials and Methods

S1.1 Data inputs

A comprehensive zoning process requires various types of physical, environmental, economic, and energy data in both specific spatial and non-spatial formats. We relied on a combination of global or continental default spatial data (Table S2) and country-provided datasets. The former serve the purpose of filling in missing country data and provide spatial uniformity for critical physical characteristics (e.g., elevation, wind speed). Country-specific datasets ensure consistency with similar past and ongoing national efforts, and in some cases, greater accuracy. We collected these data for 21 participating countries in the Eastern and Southern Africa Power Pools through a combination of stakeholders and country contacts at government agencies, utilities, and industries. The full zoning analysis could not be completed for Libya and Djibouti (both part of the Eastern Africa Power Pool) because these countries lacked requisite country-specific datasets (e.g., transmission infrastructure). As a result, we examined the Southern Africa Power Pool in more detail for the site selection process, using countries for which we could collect both transmission and demand data.

Data access Nearly all globally datasets in Table S2 are freely available and downloadable using the website links provided. LandScan (gridded global population density) and Vaisala's hourly wind data are the two exceptions, but data may be purchased by contacting the vendor directly via the website links provided. A free and open source alternative to LandScan is Worldpop (http://www.worldpop.org.uk/). Hourly demand data and transmission or substation data were acquired for each country individually. Data availability and sources are tabulated for each country in Appendix A of the MapRE report [1] and Table S5.

S1.2 Project opportunity area and zone criteria estimates

S1.2.1 Human Footprint Score

The Human Footprint Score is a metric for degree of human influence in a defined land area, and it is used in this study as a proxy for degree of human "disturbance" from natural, unaltered states [2]. We estimated this metric following Sanderson et al.'s (2002) methods [2], using the following datasets that indicate the degree of human influence and access: population density, land use/land cover, road and railway access, and surface water (rivers and oceans). Datasets were coded into standardized scores ranging from 0 (least influenced) to 10 (most influenced) (Table S4). We did not include the power infrastructure criteria in Sanderson et al. (2002), which relies on nighttime light visibility spatial data. Assumptions about electric power infrastructure's use as a proxy for population distribution and correlation with human settlements is based on developed countries' widespread electricity availability, which is not the case for many parts of our study region.

We summed the scores for each dataset to create a Human Influence Index. These scores were normalized within global terrestrial biomes [3], since absolute scores in one ecoregion may have a different effect compared to scores in another ecoregion. Within each ecoregion, the lowest Human Influence Index was assigned a Human Footprint Score of 0 and the largest index value a human footprint score of 100. The resulting Human Footprint Score represents the relative human influence within an ecoregion as a percentage of the maximum value. For example, a score of 1 within the Central Zambezian Miombo woodlands suggests that the area is the top 1% least disturbed or most wild area within the ecoregion. Since we calculated the

human footprint score for each 500 m grid cell, we averaged the scores across every grid cell in each project opportunity area.

S1.2.2 Capacity factor estimation

Solar PV To estimate solar PV capacity factors (r_{solar}), we extracted and spatially averaged the resource quality (q) (solar irradiance W/m^2) of each project opportunity area for solar PV (Eq. 1). Since land use factors that we applied are specified for MW$_{\text{ac}}$, we further applied outage rates (η_o), and inverter and AC wiring efficiencies (η_ι) to estimate the capacity factor for solar PV (Table S6). We assume an incident power density of 1000 W/m^2 to produce an output at the rated capacity of the plant.

$$r_{solar} = \frac{(1-\eta_o)\,(1-\eta_\iota)\,q}{1000} \tag{1}$$

Solar CSP Apart from the type of collector technology (parabolic trough, compact linear Fresnel reflector or heliostat solar tower), the capacity-based land use factor (e.g., MW/km^2) of solar CSP depends on two interdependent variables: the solar multiple and thermal storage. The design capacity of the solar CSP plant is based on the design output of the power turbine block. The solar multiple is the ratio of the actual size of the power plant's solar field to the size of the solar field that would be required to drive the turbine at its nominal design capacity assuming standard solar irradiance of 1 kW/m^2 at standard temperature and pressure.

Thermal storage can significantly improve the capacity factor of the plant and its ability to generate when the value of electricity is greatest, which is the greatest advantage of thermal storage. Thermal storage can enable a CSP plant to store heat during high solar insolation hours and generate electricity during the evening, night or other hours when the sun is not shining. Power plants with thermal storage can have solar multiples of up to 3-5 [4]. While such plants have a higher cost per MW due to the additional thermal storage equipment and a larger solar field (i.e., higher solar multiple), they have higher capacity factors compared to plants without thermal storage. CSP plants with no storage are typically designed to have a solar multiple between 1.1 – 1.5 [4], which is greater than 1 in order to generate electricity during the morning and evening hours when insolation is lower than threshold requirements, at the expense of losing some excess energy during the peak sun hours.

More thermal storage results in higher capacity factors (CF), but it reduces the land use factor (MW/km^2) due to the increasing solar multiple required. Given the near linear trade-off between thermal storage and land use factor, the generation-based land use factor (MWh/km^2) should be invariant to thermal storage assumptions. Nonetheless, we estimate CFs assuming both storage and no storage. Due to lack of empirical land use factor data for thermal storage systems, we use average empirical land use factors for no-storage CSP plants examined in the USA, which are more robust (as measured by number of data samples), and applied the ratio of storage to no-storage solar multiples to estimate land use factors for CSP plants with thermal storage (Table S6) [5].

Models of CSP power plant generation are complex and difficult to approximate using only design calculations and average direct normal insolation (DNI) values. Instead, we used the National Renewable Energy Laboratory's System Adviser Model [6] to simulate the CF for 45 locations throughout the study region in Africa and five locations in California and Arizona (in order to achieve greater representation of higher DNI regions) for two generic CSP plants with the following assumptions: (1) no storage and a solar multiple of 1.2; (2) 6 hours of storage and a solar multiple of 2.1. Weather data for both U.S. and African locations were available from the U.S. Department of Energy Simulation Software database, a compilation of weather

data from multiple sources [7]. We linearly regressed each location's CF against its DNI, wind speed, temperature, and latitude, and determined that DNI was the only statistically significant explanatory variable for trends in CF. We plotted CF against DNI and chose to fit a logarithmic equation to the data because of known increased efficiency losses at the higher end of the DNI range (Figure S6). We used these fitted equations (Figure S6) to estimate the CF for the spatially averaged DNI in each project opportunity area for both no-storage and 6-hr-storage CSP power plant design assumptions.

Wind The capacity factor of a wind turbine installation depends on the wind speed distribution at the wind turbine hub height, the air density at the location, and the power curve of the turbine. We used spatially-averaged shape and scale parameters for the Weibull distribution provided by 3Tier Inc. (now Vaisala Inc.) to generate a wind speed probability distribution per 3.6 km grid cell (the resolution of 3Tier data).

Air density is inversely related to elevation and temperature. It decreases with increasing elevation or temperature, and as a result, can significantly affect the power in the wind for a particular wind speed regime. Wind turbine power curves provided by manufacturers typically assume an air density of 1.225 kg/m^3, which is the air density at sea level and 15^{o}C. An increase in elevation from sea level to 2500 m can result in 26% decrease in air density. Changes in temperature produce a smaller yet significant effect on air density compared to elevation. A temperature increase from 0^{o}C to 25^{o}C can result in a drop of 8% in air density. To account for the effect of air density on power generation, we first estimated the air density for each grid cell, and then applied power curves modified for different air densities to the wind speed distributions.

For air density, we first estimated the pressure (p) for each grid cell from the elevation and temperature of those grid cells (see Table S2 for data sources), the air pressure at sea level (p_o: 101325 Pa), the gravitational acceleration (g: 9.807 kg/m^3), and the gas constant (R: 287.04 J/kg-K) (Eq. 2) [8]. We then estimated the air density (ρ) from the estimated pressure (p), the gas constant and temperature of the grid cell (Eq. 3).

$$p = \rho \cdot e^{\frac{-Zg}{RT}} \tag{2}$$

$$\rho = \frac{p}{RT} \tag{3}$$

On-shore wind turbines are generally classified into three International Electrotechnical Commission (IEC) classes depending on the wind speed regimes. We used normalized wind curves for the three IEC classes developed by the National Renewable Energy Laboratory [9] (see Figure S7), and scaled these to a 2000 kW rated wind turbine. Adopting an approach similar to [10], we assumed the IEC Class III and II turbines to be viable in sites up to the reference wind speeds of 7.5 m/s and 8.5 m/s respectively, as defined by the IEC. For sites with average wind speeds above 8.5 m/s, we assumed the IEC Class I turbine to be suitable. In reality, depending on the site-specific gust, turbulence, and air density, IEC Class II and III turbines could be placed at sites with higher average wind speeds than those assumed in our analysis, in order to extract more energy from the wind [10].

For each of the three turbine classes, we adjusted the power curves for a range of air densities by scaling the wind speeds of the standard curves according to the International Standard IEC 61400-12 [11] [12]. In Equation 4, v_{adj} is the adjusted wind speed, v_{std} is the wind speed from the standard power curve, ρ_{std} is

the standard air density of 1.225 kg/m^3, and ρ_{adj} is the estimated air density of the grid cell.

$$v_{adj} = v_{std} \left(\frac{\rho_{std}}{\rho_{adj}} \right)^{1/3} \tag{4}$$

Since the resulting power curve (v_{adj}, P_{std}) is evaluated at the adjusted wind speed values, v_{adj}, we needed to interpolate the P_{adj} at discrete wind speed values (v_{std}) in order to plot the air-density-adjusted power curve (v_{std}, P_{adj}) [12]. The resultant adjusted power curves show that air density can significantly affect the wind turbine power curves, and subsequently, the expected capacity factors at a site (Figure S8).

To compute the capacity factor for each 3.6 km grid cell, we selected the appropriate air-density-adjusted power curve given the average wind speed, which determines the IEC class, and the air density, which determines the air-density adjustment within the IEC class. For each grid cell, we then discretely computed the power output at each wind speed given its probability (determined by the Weibull distribution parameters provided by 3Tier) and summed the power output across all wind speeds within the turbine's operational range to calculate the mean wind power output in W ($\overline{P}$). The capacity factor (r_{wind}) is simply the ratio of the mean wind power output to the rated power output of the turbine (P_r or 2000 kW), accounting for any collection losses (η_a) and outages (η_o) (Eq. 5).

$$r_{wind} = \frac{(1 - \eta_a) \cdot (1 - \eta_o) \cdot \overline{P}}{P_r} \tag{5}$$

S1.2.3 Levelized cost of electricity (LCOE) calculations

The LCOE is a metric that describes the average cost of electricity for every unit of electricity generated over the lifetime of a project at the point of interconnection. Using the size (km^2) (a_x) of the project opportunity area x and its associated land use factor (l_t) for technology t, land use discount factor (f_t) for technology t, distance to nearest substation (or transmission line; $d_{i,x}$) and road ($d_{r,x}$) from area x, and economic parameters listed in Table S6, we calculated the generation, interconnection and road components of the levelized cost of electricity (LCOE in USD/MWh). Note that the size (km^2) of a project opportunity area (a) and its associated land use factor (l_t) and land use discount factor (f_t) cancel out in the LCOE equations, but are included for completeness to show the ratio of cost to electricity generation (Eqs. 6 - 8).

Road LCOE was estimated using a fixed capital cost per km of additional road needed to service the project, and is expressed per unit of electricity output from the project. Since road capital costs do not scale according to installed capacity of a project, unlike generation and interconnection costs which increase with each additional MW of capacity, the size of a project opportunity area affects the road cost. That is, a POA within 10 km of existing road infrastructure will have a higher road cost than another POA within the same distance of the nearest road if it is comparatively smaller in land area. In order to allow road LCOEs to vary only by each POA's road connection distance and resource quality, we assumed 50 MW of capacity per POA regardless of size (Eq. 8). We assumed that one road will be built for every 50 MW capacity project, which is a reasonable size for a utility-scale project, and roughly equal to the potential capacity of a project opportunity area.

Total LCOE is simply the sum of the generation, interconnection, and road cost components. We prioritize distance to nearest substation in estimating transmission LCOE when high quality spatial data for sub-

stations were available, but we also estimated transmission LCOE costs based on distance to the nearest transmission line. Refer to Table S6 for values used in LCOE calculations.

$$LCOE_{generation,t,x} = \frac{a_x l_t \left(1 - f_t\right) \left(c_{g,t} i_{cr} + o_{f,g,t}\right)}{8760 \cdot a_x l_t \left(1 - f_t\right) r_{t,x}} + o_{v,g,t} \tag{6}$$

$$LCOE_{interconnection,t,x} = \frac{a_x l_t \left(1 - f_t\right) \left(d_{i,x} \left(c_i i_{cr} + o_{f,i,t}\right) + c_s i_{cr}\right)}{8760 \cdot a_x l_t \left(1 - f_t\right) r_{t,x}} \tag{7}$$

$$LCOE_{road,t,x} = \frac{d_{r,x} \left(c_r i_{cr} + o_{f,r}\right)}{8760 \cdot r_{t,x} \cdot 50MW} \tag{8}$$

Where $c_{g,t}$ is the capital cost of generation for technology t; c_i is the capital cost of interconnection (i); c_s is the capital cost of substation (s); c_r is the capital cost of road; $r_{t,x}$ is the capacity factor of technology t and area x; $o_{f,g,t}$ is the fixed operations and maintenance cost of generation for technology t; $o_{f,i,t}$ is the fixed operations and maintenance cost of interconnection (i) for technology t; $o_{v,g,t}$ is the variable (v) operations and maintenance cost of generation (g) for technology t; $o_{v,i,t}$ is the variable (v) operations and maintenance cost of interconnection (i) for technology t; $o_{f,r}$ is the fixed (f) operations and maintenance cost of roads (r). The capital recovery factor (i_{cr}) converts a present value to a uniform stream of annualized values given a discount rate and the number of interest periods (Eqn. 9). We have assumed a real discount rate (i) of 10% that reflects the high cost of capital in Africa. n is the number of years in the lifetime of a power plant.

$$i_{cr} = \frac{i \left(1 + i\right)^n}{\left(1 + i\right)^n - 1} \tag{9}$$

Although LCOE assumptions were selected to be as representative of current conditions and costs, these LCOE estimates are best used to compare costs within a single technology since LCOE values may be higher or lower than others reported in the literature given the dynamic nature of the industry. Further, the discount rate can significantly affect the LCOE, and can vary across countries.

System integration costs or balancing costs are not included in LCOE estimates. These can vary across countries based on their electricity generation mix. For example, hydro capacity with storage is considered more flexible than coal power plants that typically incur a higher penalty for cycling in order to balance both variable renewable energy and load (net load).

The LCOE does not account for differences in the value of electricity generated by different technologies in a particular location. Generation at different times of the day or year have different economic value depending on the demand and the available generation at that time.

LCOE estimates are based on present existing and planned transmission and road infrastructure. In this study, we did not value a project opportunity area sequentially based on the utilization of infrastructure that may be built earlier for another nearby planned project.

S1.3 Wind build-out scenario analysis

S1.3.1 Input load and wind generation data

We created load profiles for the year 2030 ($d_{2030,t}$) using the projected annual demand in 2030 [13], [14] by multiplying the load in each hour t ($d_{2013,t}$) by the ratio of the 2030 annual load (D_{2030}; Table S7) to the 2013 annual load (Eq. 10). This simple load projection technique assumes that load profile shapes will remain the same between 2013 and 2030, with an equal proportional increase in energy demand across all hours. See section S1.3.4 for methods used to conduct a sensitivity analysis of load profiles.

$$d_{2030,t} = d_{2013,t} \frac{D_{2030}}{\sum_{t=1}^{T} d_{2013,t}} \tag{10}$$

For the Southern Africa Power Pool (SAPP) countries, we procured mesoscale modeled hourly wind generation profiles for each of 233 wind locations, selected within zone extents based on resource abundance, resource quality, representation across countries, and spatial representation within a country. Using these profiles, we created hourly capacity factor ($c_{z,t}$) profiles for all 738 wind zones in the SAPP by adjusting the hourly wind capacity factor ($c_{m,t}$) of the mesoscale modeled profile using the ratio of zones' ($\overline{c_z}$) and modeled ($\overline{c_m}$) profiles' annual average capacity factors (Eq. 11). We matched each zone to the nearest location for which we acquired mesoscale modeled wind profiles.

$$c_{z,t} = c_{m,t} \frac{\overline{c_z}}{\overline{c_m}} \tag{11}$$

S1.3.2 *Min-net-demand* site selection approach

To select wind zones and the amount of capacity to install in each zone (x_z), we minimized the maximum hourly net demand, or the difference between the hourly load and the hourly wind generation (Eq. 12). This hourly net demand is the amount of energy non-wind generators would need to supply each hour. Therefore, the maximum hourly net demand within a year is the amount of non-wind installed capacity that must be available to ensure that demand is met across all hours of the year. The objective function (Eq. 12) was minimized subject to installing a specified amount of wind capacity across the region or country (Eq. 13) (Table S7) and selecting no more than the available potential capacity of each zone (Eq. 15). We used the projected 2030 demand (Table S7) to calculate the target wind capacity (i), assuming wind will generate 30% of total annual electricity demand and have an average capacity factor of 30%. The resulting target installed capacity (i) of 61 GW across all of SAPP was consistent across scenarios.

The integer optimization problem was programmed in Python using the Pyomo module and solved using IBM CPLEX. We used this optimal wind site selection method for the following four scenarios: 30% wind penetration for each country in SAPP using only domestic wind zones (*Isolated* scenario), and 30% wind penetration across the entire SAPP region (*Interconnected* scenario), and the *Isolated* and *Interconnected* scenarios using only the top 50% of zones across three selection criteria (see the results section of the main text).

Linear optimization

Indicies

z	Zone identifier $\in \{z...Z\}$
t	Hour $\in \{1, ..., 8760\}$

Variables

x_z	Capacity to install (MW) in zone z

Parameters

$c_{z,t}$	Capacity factor of zone z hour t
$d_{2030,t}$	Electricity demand (MWh) of hour t in year 2030
p_z	Potential installed capacity (MW) of zone z
i	Target capacity (MW)

Objective function

Minimize

$$max(d_{2030,t} - \sum_{z=1}^{Z} c_{z,t} x_z) \tag{12}$$

Constraints

Subject to

$$\sum_{z=1}^{Z} x_z = i \tag{13}$$

$$x_z \geq 0 \quad \forall z \in \{z, ..., Z\} \tag{14}$$

$$x_z \leq p_z \quad \forall z \in \{z, ..., Z\} \tag{15}$$

S1.3.3 Scenario comparisons

Peak net demand calculations. Typically, conventional generation capacity is sized to meet demand. Because wind power plants are "must-run" generators, conventional generation capacity is instead sized to meet the net demand, or the difference between the demand and amount of wind generation in each hour. Therefore, to meet demand in all hours, conventional generation capacity must equal the annual peak net demand. For the *Interconnected* scenario, the conventional generation capacity is simply the coincident peak net demand, W_c (Eq. 17), or the peak net demand calculated by adding the net demand across all countries for each hour. For the *Isolated* scenarios, both coincident and non-coincident peak net demand were calculated (Eq. 16, Eq. 17). Non-coincident net demand, W_{nc}, represents the total amount of conventional capacity across the SAPP needed if each country met its net demand separately (16). Non-coincident net demand is always greater than or equal to the coincident net demand. The difference between these two values represents the avoided conventional capacity due to interconnection alone, as opposed to the balancing of wind variability through optimal site selection. This value is represented by the gray bars ("Avoided capacity due to coincident net demand") in Fig. 3B in the main text. Therefore, the coincident

peak net demand represents the conventional capacity needed to balance the net demand due to the wind profile variability.

$$W_{nc} = \sum_{y=1}^{Y} [max(w_{y,t}) \quad \forall y \in \{y...Y\}] \tag{16}$$

$$W_c = max[\sum_{y=1}^{Y} w_{y,t} \quad \forall t \in \{1...8760\}] \tag{17}$$

where

$$w_{y,t} = d_{y,2030,t} - \sum_{z=1}^{Z} c_{y,z,t} x_{y,z} \tag{18}$$

y	country $\in \{y...Y\}$
$w_{y,t}$	net demand of country y for hour t
W_{nc}	non-coincident peak net demand across all countries in the SAPP
W_c	coincident peak net demand across all countries in the SAPP
$x_{y,z}$	Capacity installed (MW) in zone z in country y
$c_{y,z,t}$	Capacity factor of zone z hour t in country y
$d_{y,2030,t}$	Electricity demand (MWh) of hour t in year 2030 for country y

Cost difference calculations. To compare approximate system costs, we monetized differences in (1) energy needs and (2) conventional capacity needs between scenarios. For (1), we assumed that any additional energy needs would be generated using hydropower or coal technologies, using the marginal cost of electricity (Table S8). Because additional energy is needed in the *min-net-demand* scenarios and its supply curve shows that the extra energy needed is during low-net-demand or baseload hours (Fig. 3C in the main text), it is more likely that coal or hydropower, rather than natural gas, will be used to supply the extra energy required. For (2), we assumed that any extra conventional capacity needed could be met using natural gas combustion turbine (CT), hydropower, or coal (see Table S8 for cost inputs). We use the non-coincident net peak demand (see Eq. 16) to represent the needed conventional capacity. We represent cost additions or savings relative to the amortized annual capital cost of wind power, which is consistent across scenarios.

Inteconnection cost estimates. A bottom-up estimate of interconnection infrastructure costs rely on knowing the lengths and voltages of new lines. A high resolution spatio-temporal 'capacity-expansion' model of the power pool's entire power system (current and future generators, their locations, and current and future transmission availability and capacity) would be needed to generate such estimates. To approximate these interconnection infrastructure costs given the lack of access to data needed to build a power systems model, we use a top-down approach that relies on the interconnection costs reported for energy trade within the SAPP. Using the MWh of energy traded in the SAPP and the revenue from wheeling charges reported in the SAPP annual reports (`http://www.sapp.co.zw/areports.html`), we calculated the wheeling cost per MWh. These wheeling costs are \$2.46/MWh for 2014 - 2015, \$2.31/MWh for 2012-2013, and \$2.62/MWh for 2011 - 2012. [15], [16]. Wheeling is the transport of electricity from within a grid to serve demand outside of the grid. One of the central reasons for wheeling charges is to recover the capital and maintenance costs of transmission infrastructure. For each *Interconnected* wind build-out scenario, we calculated the net energy traded in the SAPP by summing the difference between wind electricity generated under the *Isolated* and the *Interconnected* scenarios for each country and halving the total amount. We applied the range of wheeling fees charged by the SAPP (\$2.31/MWh - \$2.62/MWh) to calculate the wheeling charges per scenario. We then represented the wheeling charges as percentage of the amortized annual capital cost of wind power in

order to compare interconnection costs with conventional energy and conventional capacity cost differences (see section S1.3.3 above).

S1.3.4 Load profile sensitivity analysis

We created four load growth scenarios that maintain the same level of energy consumption but differ in the load profile shapes. See Fig. S10 for each scenario's hourly load profiles averaged across each month and Fig. S11 for the load duration curve across an entire year for all four scenarios. A load duration curve is the load for each hour sorted from highest to lowest. We modified each country's load profiles separately and aggregated them to create the Southern Africa Power Pool-wide load profile. The scenarios are as follows:

- "Climate – warming": relative to baseline, peak summertime (November through March) demand increases by 5% and wintertime (May through September) demand decreases by an appropriate amount to maintain the same level of energy across the year. For most SAPP countries, the annual peak demand occurs in the winter, during the months of July or August, due to heating demand and other appliance usage. Previous studies have shown that load in South Africa is extremely sensitive to climate [17], and under likely climate change scenarios, wintertime and summertime temperatures are expected to increase [18], [19]. This scenario represents greater air conditioning load increase in response to rising summer temperatures under climate change. According to Eskom, South Africa's largest utility, air conditioning load is fairly uniformly across all day-time hours and some early evening hours. Therefore, we uniformly increased summertime load from 10:00 to 22:00 from November to March. These modifications create monthly hourly average profiles that have similar daily peak demand across the year (see Fig. S10d) and reduce the annual peak demand (see Fig. S11). Tanzania's and Mozambique's load profiles were not altered in this scenario because their load profiles do not show a seasonal pattern, unlike that of the remaining seven SAPP countries.

- "Climate – extreme warming": relative to baseline, peak summertime demand increases by 8% and wintertime demand decreases by an appropriate amount to maintain the same level of energy across the year. Like the "Climate - warming" scenario, this scenario also anticipates strong summertime warming and increased AC load. The greater increase in summertime load inverts the current, baseline seasonal trend of annual peak load occurring in the wintertime for most SAPP countries (Fig S10a) to one that shows annual peak demand occurring in the summer (Fig S10e). This has the effect of slightly reducing the annual peak demand relative to baseline, but not as significantly as in the "Climate - warming" scenario (Fig. S11).

- "South Africa - hybrid": the daily hourly profiles averaged across a month for each country are combined with that of South Africa's using 50%-50% weighted averaging. This scenario represents economic structural growth in load curves to resemble that of South Africa's (Fig. S10c and S11). Although the monthly average hourly load profiles and the load duration curve do not appear to differ from that of the baseline scenario, this is primarily because South Africa contributes 85% of the demand in the SAPP. Differences in load profiles at the country-level are more discernible.

- "Daily peak increase": Increase in daily peak hours by 5-7% across all days of the year (Fig. S10b). This scenario represents increased electrification leading to increased load from appliance ownership and usage. It also represents reduced curtailment, as load shedding typically occurs during both summer and wintertime peak hours, despite summertime peak demand being less than wintertime peak demand. According to Eskom, this is because less capacity is available in the summer due scheduled maintenance. This scenario effectively increases the annual peak demand (Fig. S11).

Each of the future load growth scenarios were generated by modifying each monthly average hourly demand profile. This was done by calculating the difference between each hour's demand and the unmodified monthly

average for that hour and then adding this difference to the growth scenario's generated monthly average for that hour.

S2 Supporting figures and tables

S2.1 SI Figures and Tables for results

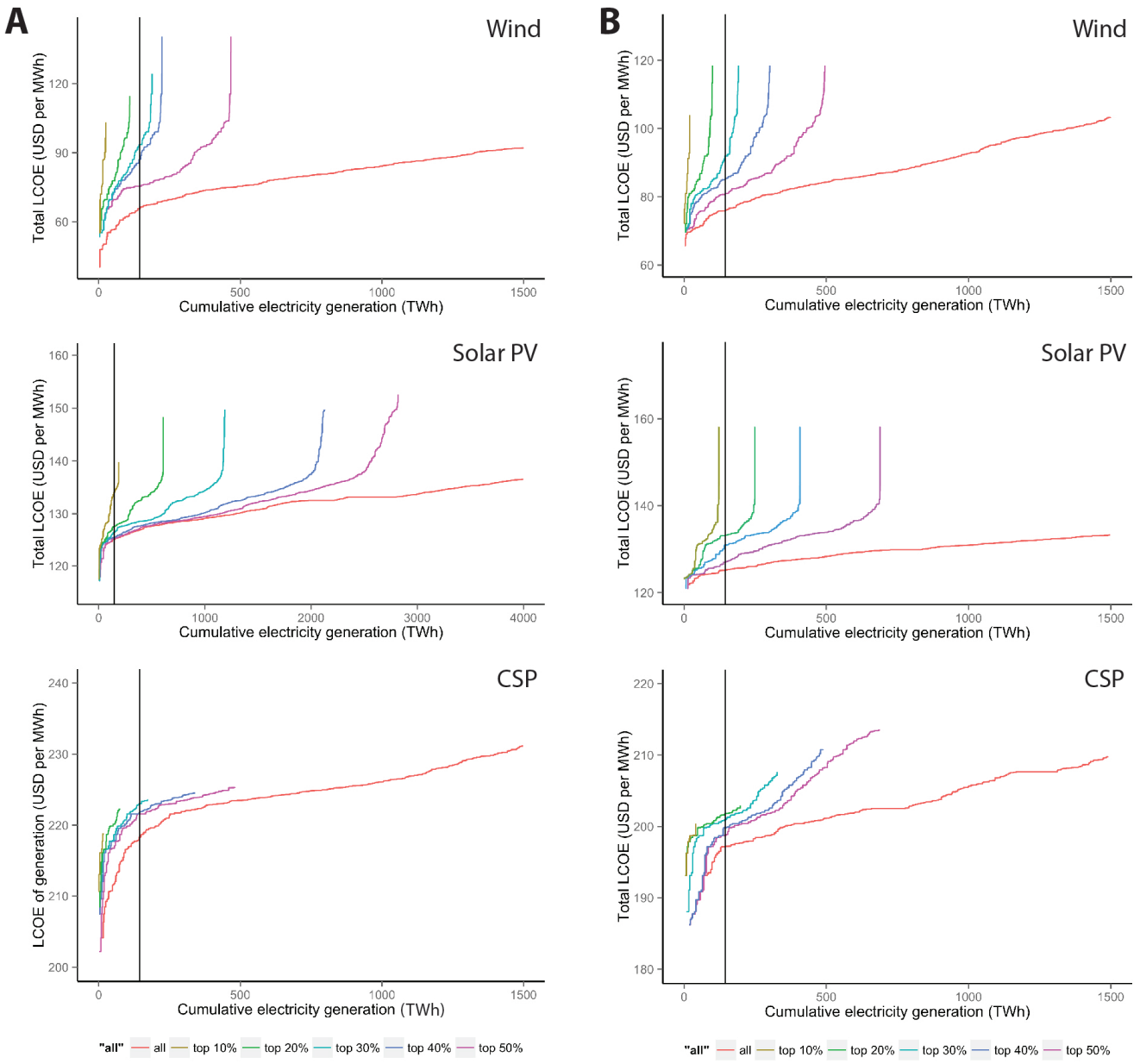

Fig. S1: ***Technology supply curves for the Eastern (A) and Southern (B) Africa Power Pools.*** *For each technology, each supply curve shows all project opportunity areas and those that meet the top 10% - 50% of siting criteria values (shortest distance to transmission infrastructure, shortest distance to load center, and greatest human footprint score). The black vertical lines show 25% of the projected demand in 2030 [13], [14]. Supply curves show whether it is possible to achieve a particular generation target in each power pool under particular levels of siting criteria constraints and at what marginal total levelized cost of electricity.*

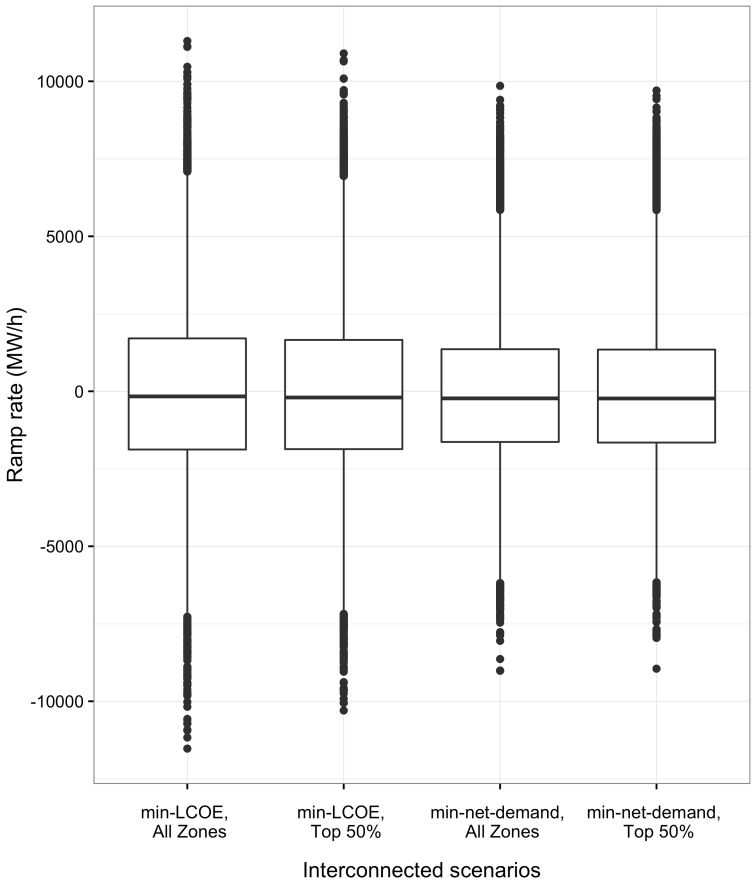

Fig. S2: ***Distribution of hourly ramp rates for the Interconnected wind build-out scenarios.*** *Ramp rates were calculated by taking the inter-hourly differences in net demand. They indicate the amount of energy that conventional generators need to produce or reduce hour-to-hour to balance the variability of wind generation. Given the range of ramp rates of conventional generators (2%/min for coal, 5% for combined cycle, and 8.3% for gas turbine [20]), 100% of available up-ramp capacity can be dispatched within an hour. If day-ahead scheduling commits enough capacity to meet the forecasted daily peak demand, there will be sufficient capacity to ramp up, regardless of the ramp requirement calculated for each scenario. However, a wider distribution of ramp rates indicates the need for more conventional generation flexibility and cycling, increasing the rate of wear-and-tear on conventional generators and increasing the system costs due to a higher demand for flexibility services.*

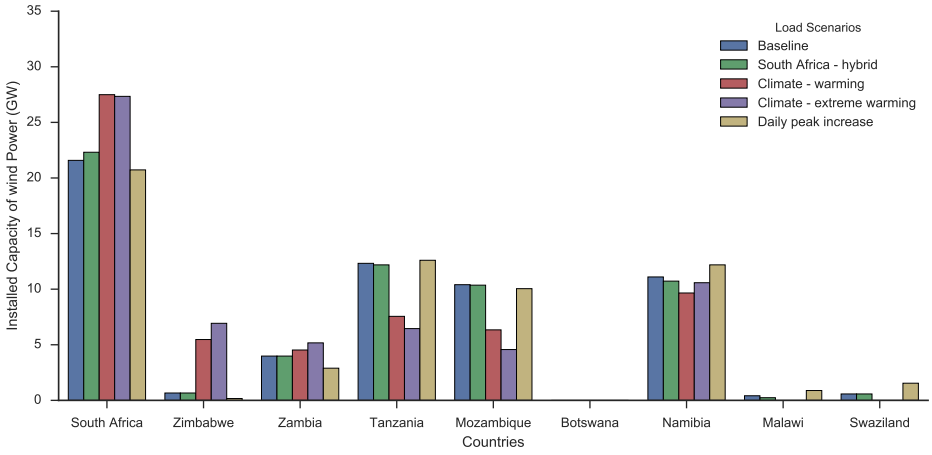

(a)

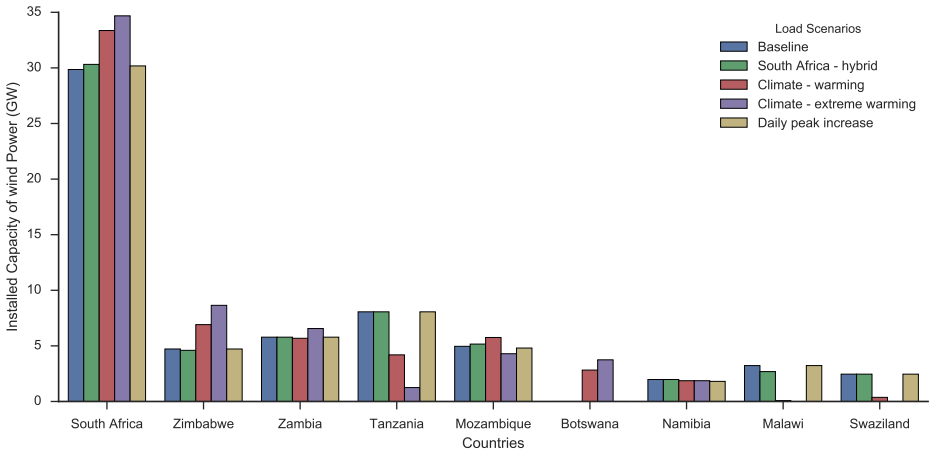

(b)

Fig. S3: Distribution of installed wind capacity among countries in the SAPP using the baseline load profile and four future load growth profiles for "Interconnected, min-net-demand, all zones" (a) and "Interconnected, min-net-demand, top 50%" scenarios (b). See Figure S10 and S11 and section S1.3.4 for descriptions of future load growth profiles.

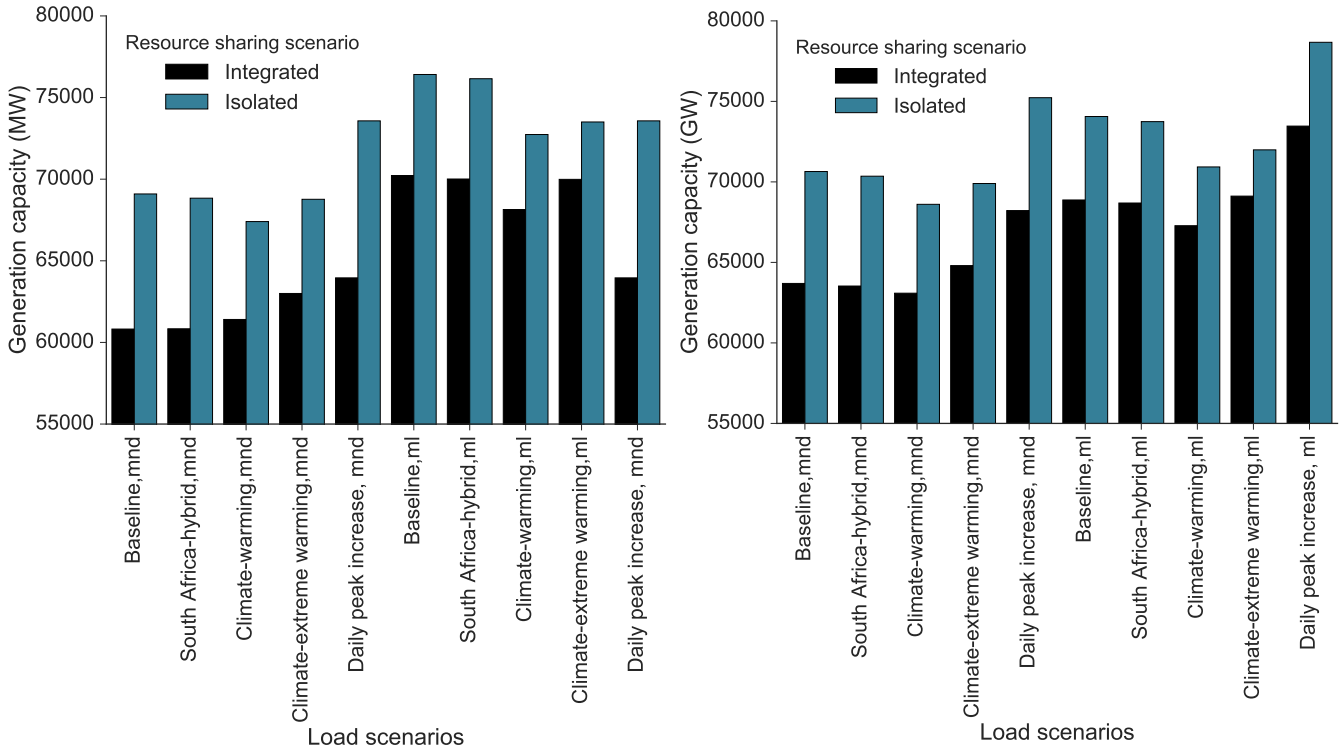

Fig. S4: Conventional installed capacity needed to meet the highest hourly net demand within a year using baseline load profiles and four load growth projections for "all zones" (a) and the "top 50%" of zones (b). Note that the range of the y-axis does not begin at zero in order to highlight the differences between scenarios. See Figures S10 and S11 for details on the load growth scenarios. "mnd" = "min-net-demand" and "ml" = "min-LCOE".

Table S1: Transmission costs for "Interconnected" wind build-out scenarios

Scenario	**Annual wheeling fees (Million USD)**	**Wheeling fees as percentage of annual wind capital costs**	**Fraction of wind energy traded**	**Net energy traded (TWh)**
Min-net-demand, all zones	210 - 240	1.6 - 1.8%	40.4%	91
Min-net-demand, top 50% zones	140 - 160	1.0 - 1.2%	28.2%	60
Min-LCOE, all zones	52 - 59	0.40 - 0.44%	9.1%	23
Min-LCOE, top 50% zones	42 - 48	0.32 - 0.36%	8.2%	18

S2.2 SI Figures and tables for methods

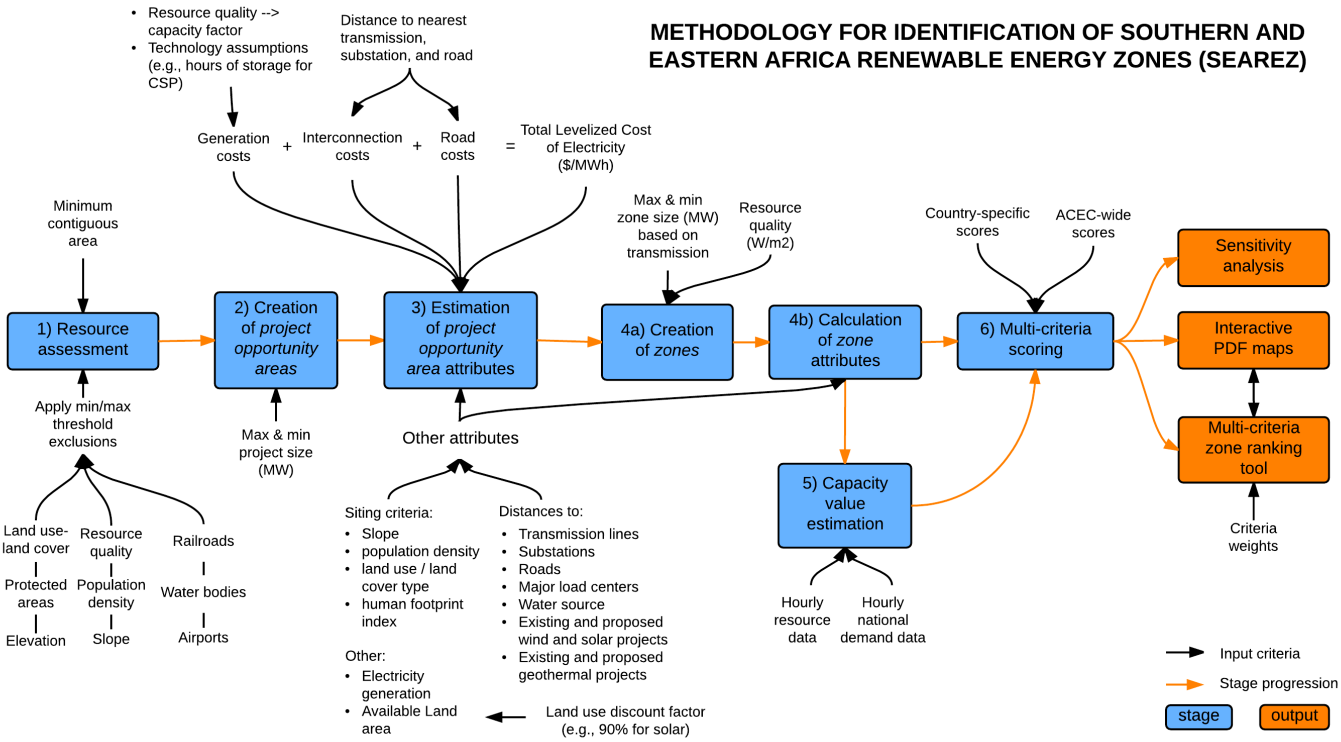

Fig. S5: ***The MapRE zoning methodology flow chart.*** *The chart shows the stages of analysis and the required inputs. Interactive PDF maps and zone ranking tool outputs are available on http://mapre.lbl.gov.*

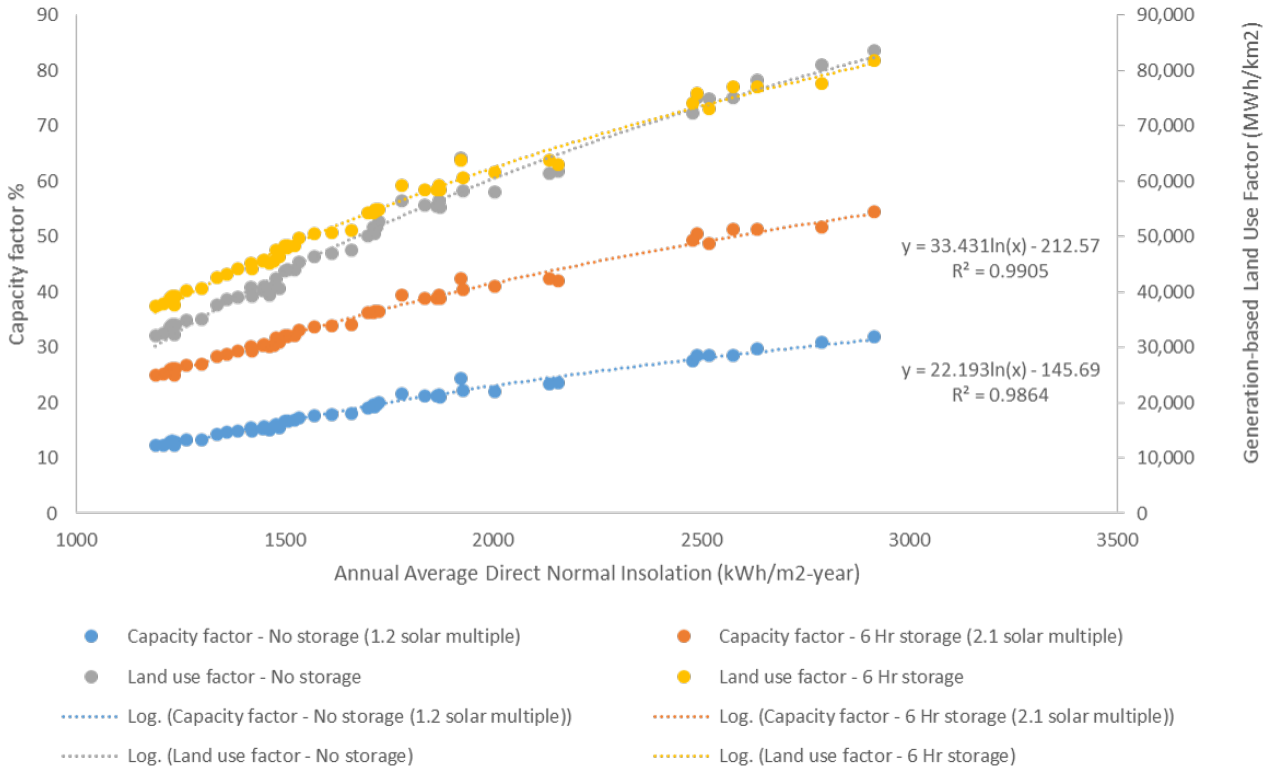

Fig. S6: Relationship between capacity factor, land use factor, and Direct Normal Insolation (DNI) for CSP. Capacity factors were simulated using specifications for a generic CSP plant in the National Renewable Energy Laboratory's System Adviser Model for 45 locations throughout the study region in Africa and five locations in California and Arizona, USA. Logarithmic equations were fit to the simulated capacity factor data to statistically model the relationship between capacity factor and DNI. Land use factors (MW/km^2) on the secondary axis were estimated for each location's capacity factor assuming an installed capacity land use efficiency of 30 MW/km^2 for no storage and 17 MW/ km^2 for 6 hours of storage.

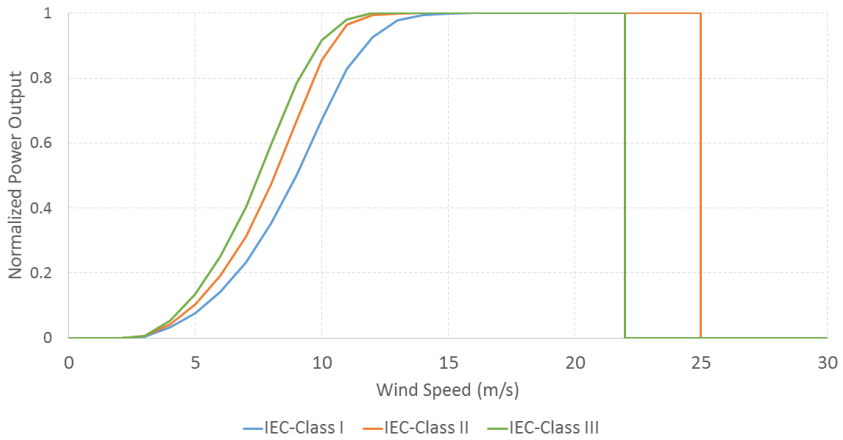

Fig. S7: Normalized wind turbine power curves for different IEC class turbines reproduced from [9].

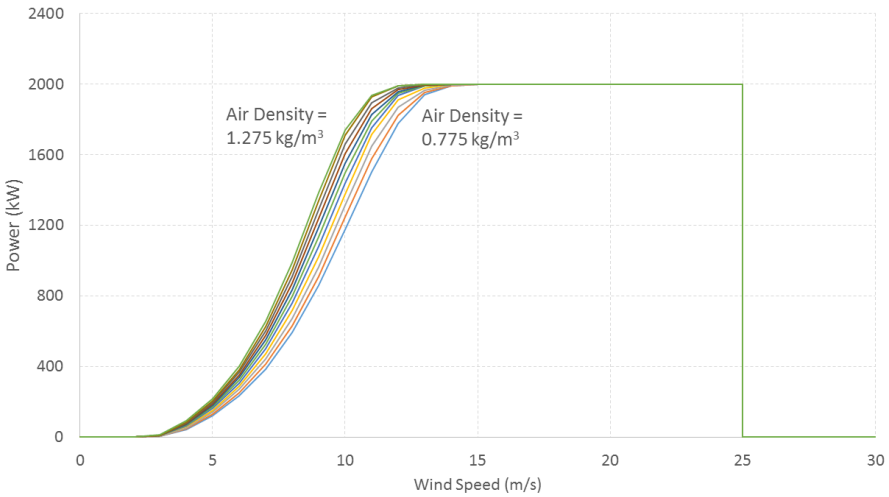

Fig. S8: Adjusted IEC Class II turbine wind power curves for air densities ranging from 1.275 kg/m^3 to 0.775 kg/m^3 (from left to right, respectively).

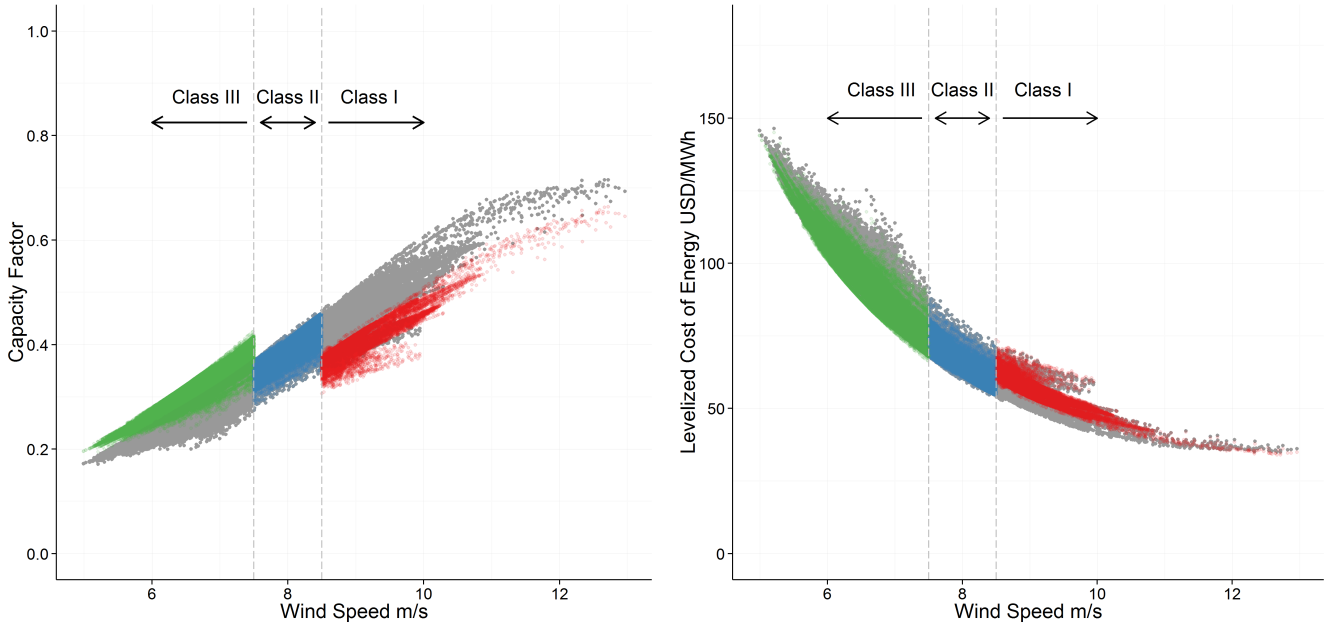

(a) *(b)*

Fig. S9: Relationship between average wind speed and estimated capacity factor (A) and levelized cost of energy for wind (B) across the Eastern and Southern Africa Power Pools. Capacity factors and LCOEs estimated using the wind-speed-appropriate Class I, II and III turbine power curves are represented by red, blue and green points respectively. Capacity factors and LCOEs estimated using just the Class II turbine power curve are also represented by grey points across the wind speed regimes.

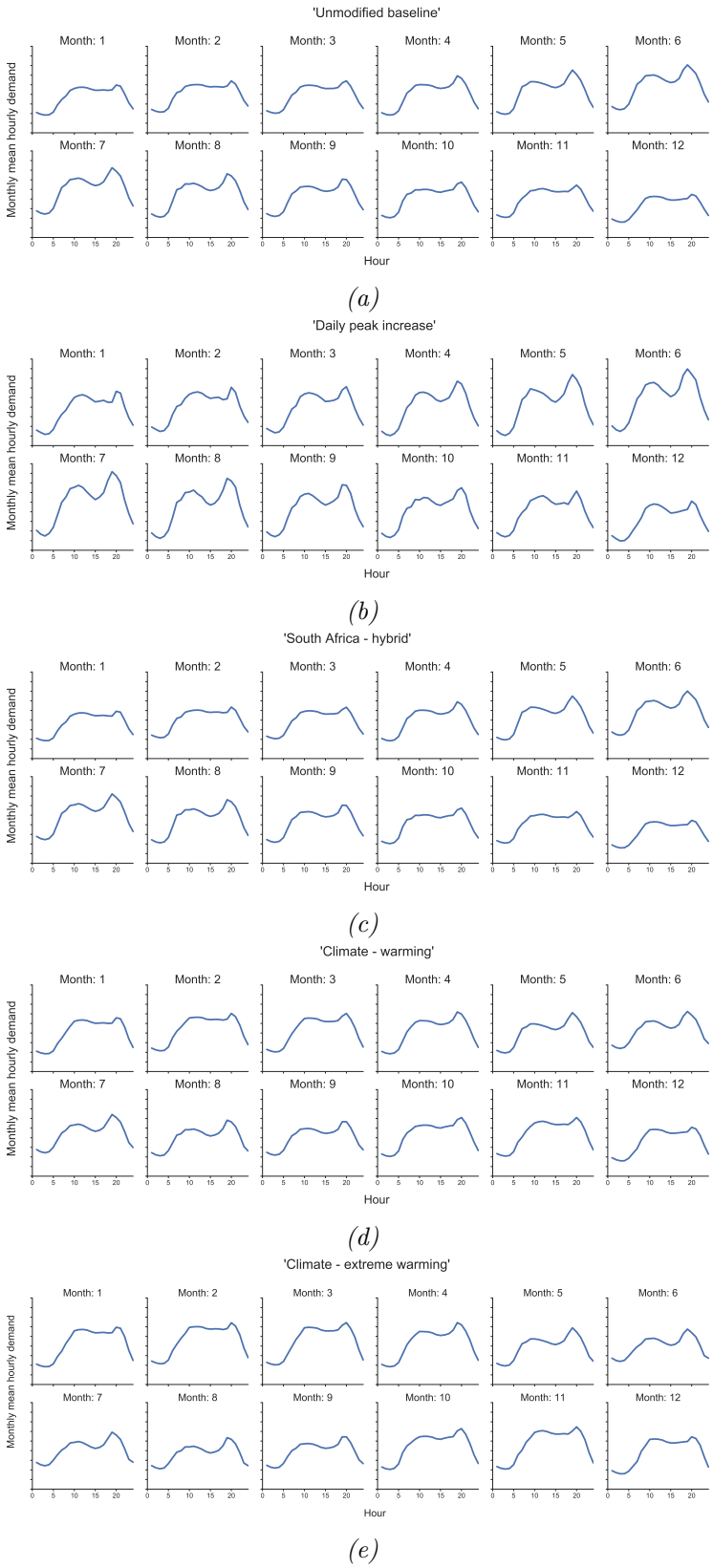

Fig. S10: Unmodified monthly mean daily load profiles of the Southern Africa Power Pool (A) and modified load profiles under the following growth scenarios: (B) increase in the daily peak hours, (C) 50% structural shift in individual country load shapes to resemble South Africa's, (D) climate warming that increases peak summertime demand by 5%, (E) climate warming that increases peak summertime demand by 8%. The total demand is the same across load growth scenarios. The y-axis of all load curves have the same scale.

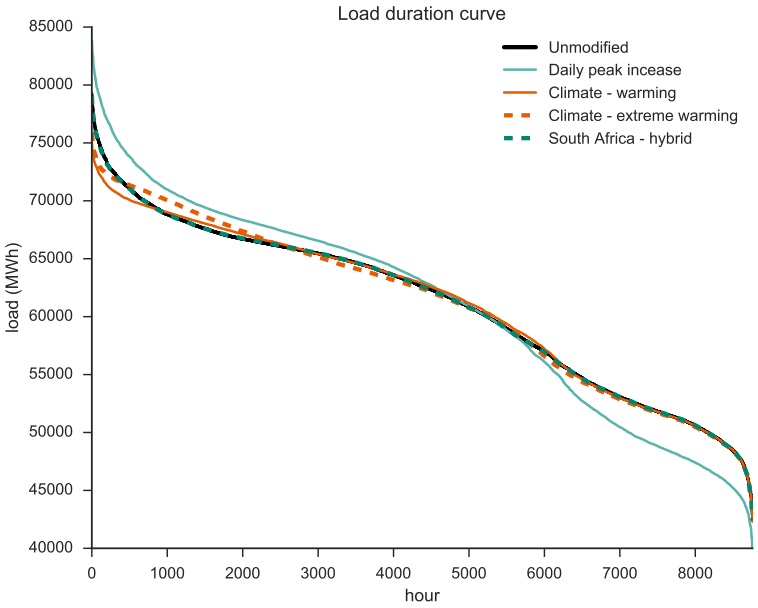

Fig. S11: ***Annual load duration curves for the Southern Africa Power Pool under various load growth scenarios.*** *A load duration curve is the load for each hour sorted from highest to lowest. "Daily peak increase" shows greater growth in the daily peak hours, "South Africa - hybrid" shows a 50% structural shift in individual country load shapes to resemble South Africa's, "Climate - warming" shows increases in peak summertime demand by 5%, "Climate- extreme warming" shows increases in peak summertime demand by 8% in countries that have seasonally varying load profiles. The total demand is the same across load growth scenarios.*

Table S2: **Data sources and resource assessment thresholds**

Stage of analysis	Category	File type	Source	Description	Year	Default exclusion thresholds
Resource assessment	Boundaries	Vector	Global Administrative Database (GADM) v2	GADM is a spatial database of the location of the world's administrative areas (or administrative boundaries) for use in GIS and similar software. Administrative areas in this database are countries and lower level subdivisions. http://www.gadm.org/country	2012	
Resource assessment	Elevation	Raster	Shuttle Radar Topographic Mission (SRTM) – CGIAR-CGI Digital Elevation dataset v4.1	Produced by NASA originally, the SRTM is a major breakthrough in digital mapping of the world and provides a major advance in the accessibility of high quality elevation data for large portions of the tropics and other areas of the developing world. 3 arc seconds (approx. 90 m) resolution. http://srtm.csi.cgiar.org/	2000	>1500 m (all technologies)
Resource assessment	Slope	Raster	SRTM - CGIAR	Created from elevation dataset using ArcGIS 10.2 Spatial Analyst.	2000	>5% (solar); >20% (wind)
Estimation of Project opportunity area attributes	Temperature	Raster	WorldClim	WorldClim is a set of global climate layers (climate grids) with a spatial resolution of about 1 square kilometer. Hijmans, R.J., S.E. Cameron, J.L. Parra, P.G. Jones and A. Jarvis, 2005. Very high resolution interpolated climate surfaces for global land areas. International Journal of Climatology 25: 1965-1978. http://www.worldclim.org/formats	1950 - 2000	
Resource assessment	Land use/land cover (LULC)	geotiff	ISGCM - Global Map V.2 (Global Version)	The Global Land Cover by National Mapping Organizations (GLCNMO) is the data of 500m (15 arc seconds) grid with 20 land cover items. The data were created by using MODIS data observed in 2008 (Terra & Aqua Satellites) with the cooperation of NMOs of the world in providing training data and validation. The classification is based on LCCS developed by FAO. Download data via: https://www.iscgm.org/gmd/	2008	See Table 2 in [1]
Resource assessment and Project oppor-tunity area attributes	Water bodies	vector	World Wildlife Federation Global lakes and wetlands database	Comprises lakes, reservoirs, rivers and different wetland types in the form of a global raster map at 30-second resolution. We excluded the following categories: lake, reservoir, river, freshwater marsh, floodplain, swamp forest, flooded forest, coastal wetland, brackish/saline wetland, and intermittent wetland/lake from. http://www.worldwildlife.org/pages/global-lakes-and-wetlands-database	2004	<500 m buffer

Stage of analysis	Category	File type	Source	Description	Year	Default exclusion thresholds
Project opportunity area attributes	Rivers	vector	Natural Earth	Natural Earth is a public domain map dataset featuring both cultural and physical vector data themes. The rivers datasets are originally from the World Data Bank 2. All rivers received manual smoothing and position adjustments to fit shaded relief generated from SRTM Plus elevation data, which is more recent and (presumably) more accurate. http://www.naturalearthdata.com/downloads/	Unknown (version 3.0.0)	
Resource assessment	Population density	raster	LandScan (Oak Ridge National Laboratory)	ORNL's LandScanTM is the community standard for global population distribution. At approximately 1 km resolution (30" X 30"), it is the finest resolution global population distribution data available and represents an ambient population (average over 24 hours). https://www.ornl.gov/ornl/careerssci/landscan/	2012	>100 persons km^{-2}
Resource assessment	Wind	raster	3Tier/Vaisala	Data were created from computer simulations using a mesoscale numerical weather prediction model and validated using publicly available wind speed observations from 194 meteorological stations within Africa from the National Centers for Environmental Prediction (NCEP). Annual wind speed, wind power density, and wind power output were provided at 80 m hub height and 5 km resolution for a typical meteorological year. Data can be downloaded on the Global Atlas by searching for "Vaisala Global wind dataset": http://irena.masdar.ac.ae/	10-year model run	<300 Wm^{-2}
Resource assessment	Solar DNI	raster	3Tier/Vaisala	The dataset is based on actual, half-hourly, high-resolution visible satellite imagery observations via the broadband visible wavelength channel at a 2 arc minute resolution. Data can be downloaded on the Global Atlas by searching for "Vaisala Global solar dataset": http://irena.masdar.ac.ae/	15 years	<250 Wm^{-2}
Resource assessment	Solar GHI				(July 1998 – last quarter)	<280 Wm^{-2}
Resource assessment	Protected Areas	vector	World Database of Protected Areas (WDPA)	The World Database on Protected Areas (WDPA) is the most comprehensive global spatial dataset on marine and terrestrial protected areas available. The WDPA is a joint project of UNEP and IUCN, produced by UNEP-WCMC and the IUCN World Commission on Protected Areas working with governments and collaborating NGOs. Download data via https://www.protectedplanet.net/	2014	<500 m buffer
Resource assessment	Protected Areas	vector	Protected Planet	Open source database that includes most WDPA locations, but also include polygon representations of the WDPA point locations (those with unknown extents/boundaries). Download data via https://www.protectedplanet.net/	2014	<500 m buffer

Stage of analysis	Category	File type	Source	Description	Year	Default exclusion thresholds
Resource assessment	Rail	vector	Africa Infrastructure Country Diagnostic (AICD) - Africa Development Bank (AfDB) and World Bank (WB)	Primary data collection efforts covering network service infrastructures (ICT, power, water & sanitation, road transport, rail transport, sea transport, and air transport) from 2001 to 2006 in 24 selected African countries. Download data via: http://www.infrastructureafrica.org/about	Variable; compiled 2011	<500 m buffer
Project opportunity area attributes	Roads	vector	AICD – AfDB and WB	See above rail category	Variable; compiled 2008	
Project opportunity area attributes	Roads	vector	gROADSv1 - Columbia University	Global Roads Open Access Data Set, Version 1 was developed under the auspices of the CODATA Global Roads Data Development Task Group at Columbia University. The data set combines the best available roads data by country into a global roads coverage, using the UN Spatial Data Infrastructure Transport (UNSDI-T) version 2 as a common data model. Download data via: http://sedac.ciesin.columbia.edu/data/set/groads-global-roads-open-access-v1	Variable; compiled 2010 (1980-2010)	
Project opportunity area attributes	Transmission	vector	AICD – AfDB and WB	Transmission lines were only available for a subset of sub-Saharan African countries. In some cases, lines do not represent geographic footprint of transmission lines but are schematics depicting points of interconnection. See Appendix A of the MapRE report [1] for transmission infrastructure data sources for each country.	Variable - compiled 2010	
Project opportunity area attributes	Renewable energy locations	vector	AICD – AfDB and WB, Cross Border Information	Existing and proposed power plants for select sub-Saharan African countries where data were available.	Variable; compiled 2011	
Project opportunity area attributes	Load centers	Lat-long coordinates	Geonames	The GeoNames geographical database is available for download free of charge under a creative commons attribution license. It contains over 10 million geographical names and consists of over 9 million unique features including 2.8 million populated places and 5.5 million alternate names. Download data via www.geonames.org	2014	
Project opportunity area attributes	Wind speed time series	.csv	3Tier/Vaisala	Hourly wind speed, wind power density, and wind power output for 10 years (same simulated data that was used to create the typical meteorological year (TMY) average values); approximately 5 km resolution. Data must be purchased from Vaisala directly: http://www.vaisala.com/en/energy/Pages/default.aspx	10-year model run	

Table S3: Adjusted resource quality thresholds for each country.

Country	**Wind W/m²**	**Solar PV GHI W/m²**	**Solar CSP DNI W/m²**	**Elevation**	**Slope**	**Population**	**LULC**
Angola	200 (lower)[1]	250 (PP)[2]	280 (PP)				
Botswana	200 (lower)	250 (PP)	280 (PP)				
Burundi	200 (lower)	230 (lower)	260 (lower)	2500 m	20% (wind and solar)	200 persons per km2	Include "Tree Open" category
DRC	200 (lower)	210 (PP)	260 (lower)	2500 m			
Djibouti	300 (PP)	250 (PP)	260 (lower)				
Egypt	200 (lower)	230 (lower)	270 (lower)				
Ethiopia	200 (lower)	250 (PP)	280 (PP)	3000 m			
Kenya	250 (lower)	250 (PP)	270 (lower)	2500 m			
Lesotho	200 (lower)	250 (PP)	280 (PP)	2500 m			
Libya	300 (PP)	250 (PP)	280 (PP)				
Malawi	200 (lower)	240 (PP)	260 (lower)	2500 m			
Mozambique	200 (lower)	230 (PP)	260 (lower)				
Namibia	200 (lower)	250 (PP)	280 (PP)				
Rwanda	200 (lower)	230 (lower)	260 (lower)	2500 m	10% (wind)	200 persons per km2	Include "Tree Open" and "Mixed Cropland" categories
South Africa	300 (PP)	250 (PP)	280 (PP)	2000 m			
Sudan	250 (lower)	250 (PP)	280 (PP)				
Swaziland	250 (lower)	210 (lower)	260 (lower)				
Tanzania	250 (lower)	250 (PP)	280 (PP)	2000 m			
Uganda	200 (lower)	250 (PP)	260 (lower)	2500 m			
Zambia	200 (lower)	250 (PP)	260 (PP)	2000 m			
Zimbabwe	200 (lower)	250 (PP)	280 (PP)				

[1]Threshold that is lower than the Power-Pool-wide (PP) resource threshold indicated in Table S2
[2]Power-Pool-wide (PP) threshold values

Table S4: Human Influence Index scoring system for Human Footprint datasets

Dataset	**Scoring system**
Population density	Score increased linearly from 0 to 10 persons/km2; all densities greater than 10 were assigned a score of 10.
Land use land cover	10 – built environments, 9 – cropland and paddy fields, 7 – cropland/mosaic vegetation, 0 – for all other land use land cover categories
Roads and railways	Areas within 1 km of roads and railways were assigned a score of 10, and those areas between 1 and 15 km assigned a score of 4.
Oceans and rivers	Areas within 1 km of rivers or the ocean oceans were assigned a score of 10, and those areas between 1 and 15 km assigned a score of 4.

Table S5: Transmission and substation spatial data availability and sources

Country	**Default transmission data**	**Country-specific substations**	**Country-specific transmission lines**
Angola	AICD[3]	N/A	N/A
Botswana	AICD	Botswana Power Corporation	N/A
Burundi	AICD	N/A	N/A
Djibouti	N/A	N/A	N/A
DRC	AICD	N/A	N/A
Egypt	CBI[4]	N/A	N/A
Ethiopia	AICD	N/A	N/A
Kenya	AICD	KETRACO	KETRACO
Lesotho	AICD	N/A	N/A
Libya	N/A	N/A	N/A
Malawi	AICD	ESCOM	ESCOM
Mozambique	AICD	Ministry of Energy	N/A
Namibia	AICD	NamPower	NamPower
Rwanda	AICD	REDC	REDC
South Africa	AICD	Eskom	Eskom
South Sudan	CBI	N/A	N/A
Sudan	CBI	N/A	N/A
Swaziland	AICD	Swaziland Electricity Company (SEC)	Swaziland Electricity Company (SEC)
Tanzania	AICD	N/A	TANESCO (partially complete)
Uganda	AICD	UNEP	UNEP
Zambia	AICD	ZESCO	N/A
Zimbabwe	AICD	ZETDC	N/A

[3]Africa Infrastructure Country Diagnostic, an African Development Bank Initiative

[4]Cross Border Information and African Energy, 2015. African Energy Atlas 2015. http://www.africa-energy.com/african-energy-atlas

Table S6: Parameters in levelized cost of electricity estimates

Parameters	**Wind**			**Solar PV**	**Solar CSP**	
					No-storage	**6 hr storage**
Land use factor [MW/km2](l)	9[1]			30[2]	30[2]	17[3]
Land use discount factor (f)	75%			90%	90%	
Costs	**Class I**	**Class II**	**Class III**		**No-storage**	**6 hr storage**
Generation – capital [USD/kW] (c_g)	1250[4]	1450[4]	1700[4]	2000[4]	3700[5]	7400[5]
Generation – fixed O&M [USD/MW/y] ($o_{f,g}$)	60000[4]			50000[4]	50000[4]	
Generation – variable O&M [USD/MWh] ($o_{v,g}$)	-			4[9]	-	
Transmission – capital [USD/MW/km] (c_i)	990[6]			990[6]	990[6]	
Transmission – fixed O&M [USD/km] ($o_{f,i}$)	-			-	-	
Substation – capital [USD / 2 substations (new transmission)] (c_s)	71000[6]			71000[6]	71000[6]	
Road – capital [USD/km] (c_r)	407000[7]			407000[7]	407000[7]	
Road – fixed O&M [USD/km] ($o_{f,r}$)	-			-	-	
Economic discount rate (i)	10%[8]			10%[8]	10%[8]	
Outage rate (h_o)	2%[9]			4%[9]	4%[9]	
Inverter efficiency and AC wiring loss (h_i)	-			4%[8]	-	
Array and collection loss (h_a)	15%[10]			-	-	
Lifetime [years] (n)	25[8]			25[8]	25[8]	

[1] Mean of U.S. empirical values (3 MW/km2) [21] and theoretical land use factors [22]

[2] [21]

[3] Estimated from no-storage land use factor by multiplying by the ratio of no-storage to 6-hr-storage solar multiples (2.1/1.2)

[4] For Class II turbine: [20]. See [23] for decrease in Class I turbine cost, and [10], [24] for increase in Class III turbine costs, relative to Class I turbine costs.

[5] [4]

[6] [20]

[7] [25]

[8] [26]

[9] Default value in the System Advisor Model (SAM) by NREL [6]

[10] [27]

Table S7: Projected 2030 electricity demand

Country	**2030 Demand (GWh)**	**Peak demand (MW)**	**Wind capacity to install by 2030 to meet 30% RPS (MW)**[5]
Angola	20294	-	N/A [6]
Botswana	7730	578	882
Burundi	622	-	N/A
Democratic Republic Of Congo	21225	-	N/A
Djibouti	764	-	N/A
Egypt	455525	-	N/A
Ethiopia	21363	-	N/A
Kenya	20646	-	N/A
Lesotho	1309	-	N/A
Libya	5420	-	N/A
Malawi	3667	475.9	419
Mozambique	8840	761	1009
Namibia	5420	546	619
Rwanda	788	-	N/A
South Africa	453069	35360	51720
Sudan	58754	-	N/A
Swaziland	1952	223	223
Tanzania	10923	898.79	1247
Uganda	9313	-	N/A
Zambia	18003	1794.6	2055
Zimbabwe	25153	1621	2871

Table S8: Cost inputs for comparing wind build-out scenarios

	Natural gas combustion turbine (CT)[7]	**Scrubbed Coal**[8]	**Hydropower**	**Wind**[9]
Capital cost ($/MW)	922,000	2,726,000	1,500,000 [10]	1450000
Fixed O&M ($/MW-yr)	5,260	31,160	15,150 [11]	60000
Variable O&M $/MWh	15.44	5	5 [12]	-
Heating value (BTU/lb)	-	10000	-	-
Fuel cost ($/MMBTU or $/MT)	-	50	-	-
Heat rate BTU/kWh	-	8800	-	-
Aux Consumption (%)	-	10	-	-
Discount rate (%)	10	10	10	10
Plant lifetime (yrs)	25	25	25	25
Marginal cost of generation ($/MWh)	-	23.2 [13]	5 [14]	-

[5] Renewable Portfolio Standard, or a target amount of renewable energy
[6] N/A: Optimal wind site selection was not performed for this country
[7] All natural gas values are from [28].
[8] All coal cost values are [28].
[9] Costs used to calculate annual amortized cost of wind capacity assume Class II turbine using values from Table S6
[10] From [29] (Figure 7.3, pg 118). This value is the average capital cost of African hydropower plants.
[11] [28]
[12] [28]
[13] Calculated using the above fuel inputs
[14] [28]

S3 Supporting references

[1] G. C. Wu, R. Deshmukh, K. Ndhlukula, T. Radojicic, and J. Reilly, "Renewable Energy Zones for the Africa Clean Energy Corridor," International Renewable Energy Agency and Lawrence Berkeley National Laboratory, LBNL#187271, Oct. 2015.

[2] E. W. Sanderson, M. Jaiteh, M. A. Levy, K. H. Redford, A. V. Wannebo, and G. Woolmer, "The Human Footprint and the Last of the Wild," *BioScience*, vol. 52, no. 10, pp. 891–904, Oct. 2002, ISSN: 0006-3568. DOI: 10.1641/0006-3568(2002)052[0891:THFATL]2.0.CO;2. [Online]. Available: http://www.bioone.org/doi/abs/10.1641/0006-3568(2002)052[0891:THFATL]2.0.CO%3B2 (visited on 03/06/2015).

[3] D. M. Olson, E. Dinerstein, E. D. Wikramanayake, N. D. Burgess, G. V. N. Powell, E. C. Underwood, J. A. D'amico, I. Itoua, H. E. Strand, J. C. Morrison, C. J. Loucks, T. F. Allnutt, T. H. Ricketts, Y. Kura, J. F. Lamoreux, W. W. Wettengel, P. Hedao, and K. R. Kassem, "Terrestrial Ecoregions of the World: A New Map of Life on Earth A new global map of terrestrial ecoregions provides an innovative tool for conserving biodiversity," en, *BioScience*, vol. 51, no. 11, pp. 933–938, Nov. 2001, ISSN: 0006-3568, 1525-3244. DOI: 10.1641/0006-3568(2001)051[0933:TEOTWA]2.0.CO;2. [Online]. Available: http://bioscience.oxfordjournals.org/content/51/11/933 (visited on 03/06/2015).

[4] IRENA, "Concentrating Solar Power - Technology Brief," International Renewable Energy Agency (IRENA), Tech. Rep., 2013.

[5] S. Ong, C. Campbell, P. Denholm, R. Margolis, and G. Heath, "Land-Use Requirements for Solar Power Plants in the United States," National Renewable Energy Laboratory, Golden, CO, Tech. Rep. NREL/TP-6A20-56290, Jun. 2013.

[6] NREL, *System Advisor Model (SAM)*, Golden, CO. [Online]. Available: https://sam.nrel.gov/content/downloads.

[7] U.S. Department of Energy, "EnergyPlus Energy Simulation Software Weather Data," Tech. Rep. [Online]. Available: http://apps1.eere.energy.gov/buildings/energyplus/cfm/weather_data2.cfm/region=1_africa_wmo_region_1.

[8] P. Gipe, *Wind Power*. 2004.

[9] J King, A Clifton, and B.-M. Hodge, "Validation of Power Output for the WIND Toolkit," National Renewable Energy Laboratory, Tech. Rep. NREL/TP-5D00-61714, Sep. 2014.

[10] R. Wiser, E. Lantz, M. Bolinger, and M. Hand, *Recent Developments in the Levelized Cost of Energy from U.S. Wind Power Projects*, 2012.

[11] IEC, *International Standard IEC 61400-12- Wind Turbine Generator Systems - Part 12: Wind turbine power performance testing*, 1998.

[12] L. Svenningsen, *Power Curves Air Density Correction and Other Power Curve Options in WindPRO*, 2010.

[13] Eastern Africa Power Pool, East African Community, SNC Lavalin International, and Parsons Brinckerhoff, "Regional Power System Master Plan and Grid Code Study," Tech. Rep., May 2011. [Online]. Available: http://eac.int/energy/index.php?option=com_docman&task=cat_view&gid=81&Itemid=70.

[14] Southern Africa Power Pool and Nexant, "SAPP Regional Generation and Transmission Expansion Plan Study," Tech. Rep., Nov. 2007.

[15] Southern Africa Power Pool, "SAPP Annual Report - 2014," Tech. Rep., 2014.

[16] ——, "SAPP Annual Report - 2015," Tech. Rep., 2015. [Online]. Available: http://www.sapp.co.zw/areports.html.

[17] D. Chikobvu and C. Sigauke, "Modelling influence of temperature on daily peak electricity demand in South Africa," *Journal of Energy in Southern Africa*, vol. 24, no. 4, pp. 63–70, Apr. 2013, ISSN: 1021-447X. [Online]. Available: http://www.scielo.org.za/scielo.php?script=sci_abstract&pid=S1021-447X2013000400008&lng=en&nrm=iso&tlng=en (visited on 10/21/2016).

[18] I. Niang, O. Ruppel, M. Abdrabo, A Essel, C Lennard, J Padgham, and P Urquhart, "Africa," in *Climate Change 2014: IMPACTS, Adaptation, and Vulnerability. Part B: REGIONAL Aspects. Contribution of Working Group II to the Fifth Assessment Report of the Intergovernmental Panel on Climate Change*, http://www.ipcc.ch/report/ar5/wg2/, Cambridge, United Kingdom and New York, NY, USA: Cambridge University Press, 2014, pp. 1199–1265. [Online]. Available: http://www.ipcc.ch/pdf/assessment-report/ar5/wg2/WGIIAR5-Chap22_FINAL.pdf.

[19] Department of Environmental Affairs, South African National Biodiversity Institute, and GIZ, *Climate Trends and Scenarios Factsheet for South Africa*, 2013. [Online]. Available: http://www.sanbi.org/sites/default/files/documents/documents/ltas-factsheetclimate-trends-and-scenarios2013.pdf.

[20] Black & Veatch Corp. and National Renewable Energy Laboratory, "Cost Estimates and Performance Data for Conventional Electricity Technologies," Tech. Rep., Feb. 2012. [Online]. Available: http://bv.com/docs/reports-studies/nrel-cost-report.pdf.

[21] S. Ong, C. Campbell, and G. Heath, "Land Use for Wind, Solar, and Geothermal Electricity Generation Facilities in the United States," National Renewable Energy Laboratory, A report from the National Renewable Energy Laboratory to the Electric Power Research Institute, Dec. 2012.

[22] Black & Veatch Corp. and RETI Coordinating Committee, "Renewable Energy Transmission Initiative (RETI) Phase 1b Final Report," Tech. Rep. RETI-1000-2008-003-F, Jan. 2009. [Online]. Available: http://www.energy.ca.gov/reti/documents/index.html.

[23] V. E. Institute, *Choice of Turbine*, 2011. [Online]. Available: http://www.vindkraft.fi/.

[24] E. Lantz, R. Wiser, and M. Hand, "IEA Wind Task 26: The Past and Future Cost of Wind Energy," National Renewable Energy Laboratory, Tech. Rep. NREL/TP-6A20-53510, 2012. [Online]. Available: http://www.nrel.gov/docs/fy12osti/54526.pdf (visited on 12/07/2014).

[25] Africon, "Africa Infrastructure Country Diagnostic: Unit Costs of Infrastructure Projects in Subsaharan Africa," Tech. Rep., 2008.

[26] IRENA, "Renewable power generation costs in 2012: An overview," International Renewable Energy Agency (IRENA), Tech. Rep., 2013.

[27] S. Tegen, E. Lantz, M. Hand, B. Maples, A. Smith, and P. Schwabe, "2011 Cost of Wind Energy Review," National Renewable Energy Laboratory, Tech. Rep. NREL/TP-5000-56266, 2013.

[28] U.S. Energy Information Administration, "Cost and Performance Characteristics of New Generating Technologies, Annual Energy Outlook 2016," Tech. Rep., Jun. 2016. [Online]. Available: http://www.eia.gov/forecasts/aeo/assumptions/pdf/table_8.2.pdf.

[29] M. Taylor, K. Daniel, A. Ilas, and E. Y. So, "Renewble Power Generation Costs in 2014," International Renewable Energy Agency (IRENA), Tech. Rep., Jan. 2015. [Online]. Available: http://www.irena.org/DocumentDownloads/Publications/IRENA_RE_Power_Costs_2014_report.pdf (visited on 08/20/2015).